SIZING AND PARAMETER STUDY OF COMPRESSOR CASE-MOUNTED PERMANENT MAGNET SYNCHRONOUS MOTOR FOR HYBRID ELECTRICAL COMPRESSOR INTEGRATION

Yinghui Yang*, Georg Möhlenkamp*

* Brandenburg University of Technology Cottbus-Senftenberg, Chair of Power Electronics and Drive Systems, Siemens-Halske-Ring 13, 03046, Cottbus, Germany

Abstract

This paper discusses the sizing and parameter estimation of a case-mounted permanent magnet synchronous motor designed for integration into a counter-rotating hybrid electrical compressor. The motor features a toroidal winding stator and a sinusoidal Halbach array permanent magnet rotor. The structure of the motor is modeled as several 2D hollow cylindrical layers for analysis and simulation. The motor model is developed with a focus on estimating parameters such as motor mass, power, and efficiency. Based on this model, a motor design algorithm is created to generate a motor design map. Serving as part of a multidisciplinary design approach, the electrical motor design map is generated as a look-up table for interfacing with other design disciplines, such as aerodynamic design, mechanical design, and propulsion system design. Therefore, motor design parameters are selected with particular emphasis on geometry and mechanical performance. The full factorial experimental method is applied to create the design map. Finally, comparative studies are conducted using the controlled variable method to analyze typical relationships between motor geometry, mass, power, efficiency, and design parameters.

KeywordsHybrid Electrical Compressor; PMSM; Parameter Study; Efficiency

NOMENCLATURE			m	Mass	[kg]
Acronyms			N	Number	[-]
AC	Alternating Current		R	Resistance	$[\Omega]$
CIPH	Cycle-Integrated Parallel Hybrid		r	Radius	[m]
CO_2	Carbon Dioxide		Re	Reynolds Number	[-]
DC	Direct Current		S	Area	$[m^2]$
PM	Permanent Magnets		T	Torque	[Nm]
PMSM	Permanent Magnet Synchronous	Motor	V	Volume	[m ³]
SHAR	Sinusoidal Halbach Array Rotor		V_r	Cylinder Rotor Volume	$[m^3]$
TWS	Toroidal Winding Stator		\mathbf{W}	Additional Parameters (Vector)	
Symbols			\mathbf{X}	Design Parameters (Vector)	
A_Z	Magnetic Vector Potential	[V·s/m]	\mathbf{Y}	Design Results (Vector)	
B	Magnetic Flux Density	[T]	δ	Resistivity	$[\Omega \cdot m]$
C,D	Coefficients in $\mathcal{A}_{\mathcal{Z}}$	[-]	μ	Permeability	[H/m]
f	Frequency	[Hz]	μ_{v}	Viscosity	[Pa·s]
H	Height	[m]	Ω	Rotational Speed	[rpm]
I	Current	[A]	ϕ	Magnetic Flux	[Wb]
J	Current Density	$[A/m^2]$	ho	Mass Density	[kg/m ³]
k	Factor/Coefficient	[-]	θ	Angle	[rad]
K_{LD}	Motor Aspect Ratio	[-]			
L	Length	[m]			

CC BY-NC-ND 4.0 i doi: 10.25967/630085

Superscripts

i Index of Region

I-VII Regions

sum Sum

Subscripts

 $egin{array}{ll} ag & {
m Air\ Gap} \\ Cu & {
m Copper} \end{array}$

dc Direct Current Component

e Eddy-current

Fe Iron

h Hysteresis

m Mechanical Component

max Maximum Value

p Particular Solution

ph Per Phase Component

pm Permanent Magnet

pp Pole Pairs

r Radial Component

rou Roughness

ry Rotor Yoke

slot Per Slot

sy Stator Yoke

T Torque

t Turns

 θ Tangential Component

v Per Unit Volume

wd Winding Wind Windage

1. INTRODUCTION

The aviation industry, a significant contributor to global carbon dioxide (CO_2) emissions, is under growing pressure to reduce its environmental impact. Electrification offers the potential to mitigate CO_2 emissions through the use of fully or partially electric propulsion systems. One innovative concept aimed at reducing emissions is the Cycle-Integrated Parallel Hybrid (CIPH) turbo-shaft engine, which incorporates electrification into either a single compressor stage or an entire compressor section [1]. In this context, a case-mounted electrical motor presents an opportunity for a tip-driven rotor stage within the compressor assembly. This configuration allows for a departure from the traditional compressor design, where each stage consists of a single rotor and stator, and introduces the possibility of a novel layout with counter-rotating rotors. This novel layout

is being investigated as part of the LuFo VI-2 "HybVer" project. One proposed concept involves driving one set of compressor rotors using the engine shaft, while the casemounted electrical motor powers another set. However, implementing such a hybrid electrified system within an aircraft engine presents practical challenges, particularly due to the limited installation space within the compressor, especially in the axial direction. Therefore, the sizing and parameter estimation of the electrical motor are critical for the successful integration of hybrid electrical compressors. Additionally, power losses in the electrical motor can lead to increased energy consumption from sources such as fuel or batteries, and contribute to an increase in overall aircraft weight. As a result, it is essential to study the motor design parameters to evaluate their impact on installation space, power output, mass, and overall efficiency in the context of hybrid electrical compressor integration.

This study specifically investigates the feasibility of a compressor case-mounted electrical motor. The chosen configuration is a Permanent Magnet Synchronous Motor (PMSM) featuring a toroidal winding stator (TWS) and a sinusoidal Halbach array rotor (SHAR). The sinusoidal Halbach array rotor provides high efficiency and power density, while the toroidal winding stator enhances the compactness of the motor design by routing the end-windings outside the stator yoke, significantly reducing the motor's length in the axial direction. In this paper, the motor structure is simplified into several 2D hollow cylindrical layers, which include key components such as the rotor voke, sinusoidal Halbach array permanent magnets, airgap, toroidal windings, and stator yoke. The motor size and mass estimation models are derived directly from geometric parameters. The motor torque and power estimation models are developed using an analytical approach based on the magnetic field distribution. The motor efficiency estimation model is formulated based on classical motor loss models, accounting for armature winding losses, core losses, and windage losses. The motor design assessment focuses on key parameters such as power output, size, mass, and efficiency. Finally, a design algorithm is introduced to explore the design space and generate a motor design map. Comparative analysis is conducted by varying motor design parameters to observe their effects on power output, mass, and efficiency. Serving as an interface with other design disciplines in the "HybVer" project, the motor design data provides essential information from the electrical drive system to support further investigations and analyses of the hybrid electrical propulsion system. Key parameters such as motor dimensions, motor mass, and motor efficiency contribute to both the design and off-design models of the propulsion system [2]. The motor's output power directly affects the degree of hybridization, which in turn influences the aerodynamic design and the overall performance of the compressor [3]. Additionally, the heat generated by motor losses, which is dissipated via the cooling system, impacts the design of the thermal management system [4].

2. METHODS

2.1. Design Objective

In this paper, the case-mounted TWS-SHAR-PMSM is represented as several 2D hollow cylindrical layers. The axial direction of the compressor is defined as the Z-axis. The cross-sectional view along the compressor axial direction is

shown in Fig. 1, and different parts of the motor are defined by their radius r as follows:

- 1) $r_1 > r > 0$: compressor (region I)
- 2) $r_2 > r > r_1$: rotor yoke (region II)
- 3) $r_3 > r > r_2$: sinusoidal Halbach array PM (region III)
- 4) $r_4 > r > r_3$: airgap (region IV)
- 5) $r_5 > r > r_4$: inner part of toroidal winding (region V)
- 6) $r_6 > r > r_5$: stator yoke (region VI)
- 7) $r_7 > r > r_6$: outer part of toroidal winding (region VII)
- 8) $r > r_7$: outer space

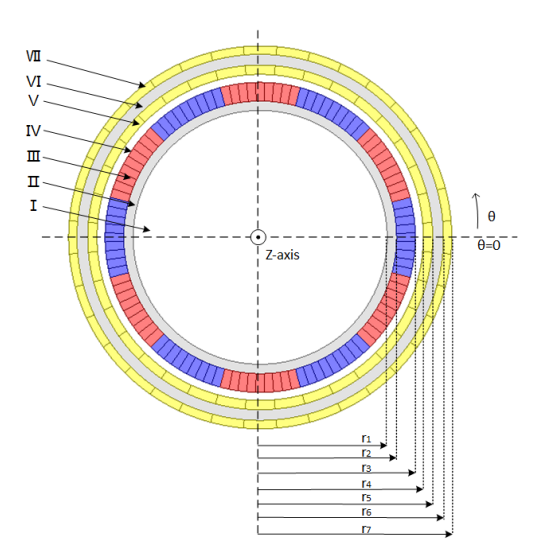


FIG 1. Cross-sectional view along the compressor axial direction of the TWS-SHAR-PMSM

The height of each hollow cylindrical layer is defined by the difference in radius as follows:

- (1) $H_{ry} = r_2 r_1$
- (2) $H_{pm} = r_3 r_2$
- (3) $H_{ag} = r_4 r_3$
- $(4) H_{wd} = r_5 r_4$
- $(5) H_{sy} = r_6 r_5$

where H_{ry} is the height of the rotor yoke, H_{pm} is the height of the PM, H_{ag} is the height of the airgap, H_{wd} is the height of the inner part of toroidal winding, and H_{sy} is the height of the stator yoke. To ensure the current density of the inner and outer toroidal windings in one phase is the same, the outer radius r_7 is related to r_4 , r_5 , and r_6 as:

(6)
$$r_7^2 - r_6^2 = r_5^2 - r_4^2$$

The cross-sectional view perpendicular to the compressor axis is shown in Fig. 2. The center dashed line represents the axial direction of the compressor. The grey region corresponds to the rotor, which consists of the rotor yoke and the permanent magnets, while the yellow region corresponds to the stator, which includes the stator yoke and toroidal windings.

To simplify the modeling and analysis, the following assumptions are made:

- 1) all parts of the motor are simplified as hollow cylinders with the same axial length *L*;
- 2) the end winding of the motor is neglected;
- 3) the rotor bandage and the stator sleeve are neglected;
- 4) the same assumptions are made as in paper [5], for the analysis of the electromagnetic field distribution;

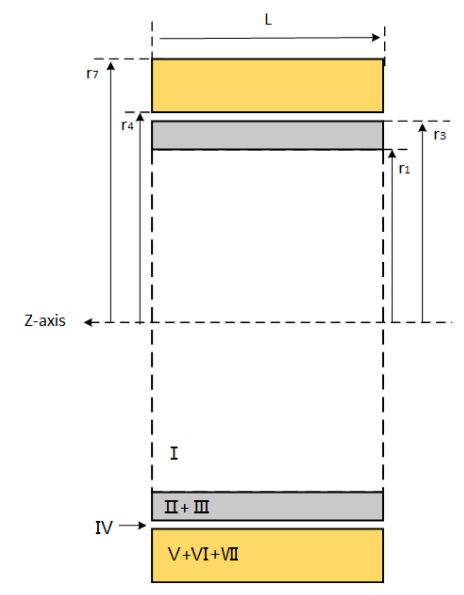


FIG 2. Cross-sectional view perpendicular to the compressor axis of the TWS-SHAR-PMSM

- 5) only a single parallel path in the stator winding;
- 6) Litz wire is used
- 7) the bearing structure is neglected;

2.2. Motor Mass Estimation Model

The total mass of the motor includes all its solid parts, namely the stator and rotor. The rotor consists of the rotor yoke (region II) and permanent magnets (region III). The stator consists of the stator yoke (region VI) and the windings (region V and region VII). All components are simplified as hollow cylinders, and the mass of each component is calculated based on its mass density and volume as follows:

(7)
$$m^{i} = \bar{\rho^{i}}V^{i} = \bar{\rho^{i}}\pi L(r_{out}^{i}{}^{2} - r_{in}^{i}{}^{2})$$
 where: $i \in \{II, III, V, VI, VII\}$

The $\bar{\rho^i}$ is the material's average mass density of each region, L is the axial length, and r^i_{out} and r^i_{in} are the outer and inner radius of each hollow cylinder, which has:

(8)
$$r_{out}^i, r_{in}^i \in \{r_1, r_2, ... r_7\}$$

With the assumed utilization of Litz wire, the slot fill factor k_{slot} is considered. Due to the slotless structure of the TWS, each copper coil is treated to occupy a virtual slot. Thus, the $\bar{\rho^i}$ of region V and VII has:

(9)
$$\bar{\rho^i} = k_{slot} \times \rho_{Cu}, i \in \{V, VII\}$$

where ρ_{Cu} is the mass density of the copper. For other regions, the material's average mass density is simplified as the mass density of the main material. The total mass of the motor is calculated by summing the masses of all relevant components:

$$(10) m^{sum} = \sum_{i} m^{i}, i \in \{II, III, V, VI, VII\}$$

2.3. Motor Power Estimation Model

iii

The analytical model of the magnetic field distribution in the TWS-SHAR-PMSM is introduced in [5]. The magnetic vec-

tor potential A_Z^i for regions III, IV, V, and VII is expressed in the cylindrical coordinate system as follows:

(11)
$$\begin{split} A_Z^i &= (C_1^i r^{N_{pp}} + C_2^i r^{-N_{pp}}) sin(N_{pp}\theta) \\ &+ (D_1^i r^{N_{pp}} + D_2^i r^{-N_{pp}}) cos(N_{pp}\theta) + A_{Zp}^i \end{split}$$
 where: $i \in \{III, IV, V, VII\}$

Here, N_{pp} represents the number of motor pole pairs. The coefficients C_1^i , C_2^i , D_1^i , and D_2^i , as well as the particular solution A_{Zp}^i , are derived from the motor parameters. From the magnetic vector potential, the magnetic field distribution is calculated as follows:

(12)
$$B_r^i = \frac{1}{r} \frac{\partial A_Z^i}{\partial \theta}, i \in \{III, IV, V, VII\}$$

(13)
$$B_{\theta}^{i}=-\frac{\partial A_{Z}^{i}}{\partial r},i\in\{III,IV,V,VII\}$$

where B_r^i and B_θ^i are the radial and tangential components of the magnetic flux density, respectively. The electromagnetic torque is calculated using the Maxwell stress tensor and is expressed as:

(14)
$$T = \frac{2\pi L N_{pp}^2 (C_1^{IV} D_2^{IV} - C_2^{IV} D_1^{IV})}{\mu_0}$$

where μ_0 is the magnetic permeability of vacuum. The mechanical power P_m is calculated from the torque and the rotational speed Ω_m as follows:

$$(15) P_m = T \cdot \frac{2\pi}{60} \Omega_m$$

2.4. Motor Efficiency Estimation Model

There are various types of losses in PMSM, including armature winding losses, armature core losses, rotor core losses, losses in the PM, rotational mechanical losses, and windage losses, among others [6]. Rotor core losses and losses in the PM are typically negligible compared to losses in the stator. Based on the assumptions made earlier, rotational mechanical friction losses are also neglected. Therefore, the main losses considered in this paper are the armature winding losses P_{Cu} , armature core losses P_{Fe} , and windage losses P_{Wind} . The motor efficiency is expressed as:

(16)
$$\eta = \frac{P_{out}}{P_{in}} = \frac{P_m}{P_m + P_{Cu} + P_{Fe} + P_{Wind}}$$

2.4.1. Armature winding losses

The armature winding losses, also known as copper losses, represent the resistance losses in the armature windings. In a three-phase motor, these losses are calculated based on the winding resistance ${\it R}$ and the winding current ${\it I}$, as follows:

$$(17) P_{Cu} = 3I^2R$$

According to [6], the armature winding resistance per phase for DC current R_{dc} is calculated based on the resistivity of copper δ_{Cu} , the average length of the armature turn L_{ph} , the cross-sectional area of copper per slot $S_{slot,Cu}$, and the number of turns per slot N_t , as follows:

$$R_{dc} = \delta_{Cu} \cdot \frac{L_{ph}}{S_{slot,Cu}/N_t}$$

Since it is assumed that there is only a single parallel path in the stator winding, the average length of the armature turn is calculated as:

$$(19) L_{ph} = 4N_{pp}N_tL$$

The copper area per virtual slot $S_{slot,Cu}$ is calculated from the area of the virtual slot S_{slot} and the slot fill factor k_{slot} , as follows:

$$(20) S_{slot,Cu} = k_{slot} \cdot S_{slot}$$

(21)
$$S_{slot} = \frac{\pi(r_5^2 - r_4^2)}{6N_{pp}}$$

The phase current is calculated based on the current density, the copper area per virtual slot, and the number of turns per virtual slot, as follows:

$$I = \frac{J \cdot S_{slot,Cu}}{N_t}$$

When the motor is driven by AC current, especially at high fundamental frequencies, AC proximity and skin-effect losses need to be considered in the armature winding losses, referred to as AC losses. According to [7], the utilization of Litz wire can significantly reduce these AC losses. Therefore, in this paper, the armature winding resistance per phase is approximated to be equal to the armature winding resistance per phase for DC current, as:

$$(23) R \approx R_{dc}$$

2.4.2. Armature core losses

The armature core losses considered in this paper include both hysteresis loss P_h and eddy current loss P_e . The per unit volume armature core losses P_v are estimated as follows [8]:

(24)
$$P_{v} = P_{h} + P_{e} = k_{h} B_{sy.max}^{2} f + k_{e} B_{sy.max}^{2} f^{2}$$

where $B_{sy.max}$ is the peak magnetic flux density in the stator yoke, k_h is the hysteresis loss coefficient, k_e is the eddy-current loss coefficient, and f is the frequency, which is calculated as:

$$(25) f = N_{pp} \frac{\Omega_m}{60}$$

Therefore, the armature core losses are estimated as:

(26)
$$P_{Fe} = P_{\nu}V^{VI} = P_{\nu} \cdot \pi L(r_6^2 - r_5^2)$$

2.4.3. Windage losses

iν

According to the paper [9], the windage losses from the rotating cylinder mantle are estimated as:

(27)
$$P_{Wind} = \frac{1}{32} k_{rou} k_T \pi \rho_{ag} (\frac{2\pi}{60} \Omega_m)^3 (2r_3)^4 L$$

where k_{rou} is the roughness coefficient, and k_T is the torque coefficient which can be obtained using equation (28) based on the Reynolds number Re.

(28)
$$k_T = \begin{cases} 10 \cdot \frac{\left(H_{ag}/r_3\right)^{0.3}}{Re} & Re < 64\\ 2 \cdot \frac{\left(H_{ag}/r_3\right)^{0.3}}{Re^{0.6}} & 64 < Re < 500\\ 1.03 \cdot \frac{\left(H_{ag}/r_3\right)^{0.3}}{Re^{0.5}} & 500 < Re < 10^4\\ 0.065 \cdot \frac{\left(H_{ag}/r_3\right)^{0.3}}{Re^{0.2}} & 10^4 < Re \end{cases}$$

CC BY-NC-ND 4.0

(29)
$$Re = \frac{\rho_{ag}r_3H_{ag}}{\mu_{\upsilon}} \cdot \frac{2\pi}{60}\Omega_m$$

where μ_{υ} is the viscosity of the air.

3. DESIGN ALGORITHM AND PARAMETER STUDY

3.1. Design Algorithm

In this paper, the motor design parameters are defined as a vector \mathbf{X} , and the motor design results are defined as a vector \mathbf{Y} .

(30)
$$\mathbf{X} = [r_1, K_{LD}, H_{ag}, H_{pm}, H_{wd}, \Omega_m, J, N_{pp}, N_t]$$

$$\mathbf{Y} = [m^{sum}, \eta, P_m]$$

In ${\bf X}$, the element r_1 represents the outer radius of the compressor, and the element K_{LD} represents the geometric shape of the motor. The motor aspect ratio K_{LD} is defined as:

$$(32) K_{LD} = \frac{L}{r_1}$$

The main design results Y include motor mass, motor efficiency, and motor power, which are the primary outputs of the motor models. All other auxiliary parameters necessary for the motor models, such as material mass density, copper resistivity, hysteresis loss coefficient, eddy-current loss coefficient, and similar properties, are defined as additional parameters W. The algorithm for the design of full factorial experiments is shown in Fig. 3, labeled as DOE in yellow. The output of this algorithm is the motor design map as a look-up table, which provides the results for various combinations of design parameters and design results.

To maintain similarity between the motors, the magnetic flux density in both the stator yoke and rotor yoke remains constant as the design parameters change. In this paper, they are designed to be 1.8T. Assuming an even distribution of the magnetic flux density in the rotor and stator yokes, the peak magnetic flux densities are estimated as:

$$B_{ry.max} = \frac{\phi_{ry}}{H_{ry}}$$

$$B_{sy.max} = \frac{\phi_{sy}}{H_{sy}}$$

where ϕ_{ry} is the per-half-pole magnetic flux in the rotor yoke, and ϕ_{sy} is the per-half-pole magnetic flux in the stator yoke. The normal component of the magnetic flux passing through the boundary of the stator and rotor yokes per half pole is calculated as:

(35)
$$\phi_{ry} = \int_0^{\frac{\pi}{2N_{pp}}} B_r^{III}|_{r=r_2} d\theta$$

(36)
$$\phi_{sy} = \int_{0}^{\frac{\pi}{2N_{pp}}} (B_r^V|_{r=r_5} + B_r^{VII}|_{r=r_6}) d\theta$$

The iterative method is employed in the design algorithm to determine the appropriate values for H_{ry} and H_{sy} . For each motor design parameter set $\mathbf{X_j}$, the values of H_{ry} and H_{sy} are initially assigned. Subsequently, the peak magnetic flux densities $B_{ry.max}$ and $B_{sy.max}$ are calculated. The deviation of $B_{ry.max}$ and $B_{sy.max}$ from the target value of 1.8T is computed as $\Delta B_{ry.max}$ and $\Delta B_{sy.max}$. If the deviation exceeds a specified threshold, which is 1mT in this paper, the

new values for H_{ry} and H_{sy} are updated by multiplying the deviation by factors c_1 and c_2 . Once the deviation falls below the threshold, the valid motor design result $\mathbf{Y_j}$ is computed. In the relation $\mathbf{Y_j} = f(\mathbf{X_j}, \mathbf{W})$, the function f represents the motor mass estimation model, the motor power estimation model, and the motor efficiency estimation model. The algorithm is illustrated in Fig. 3, where the motor model for each iterative loop is highlighted in green.

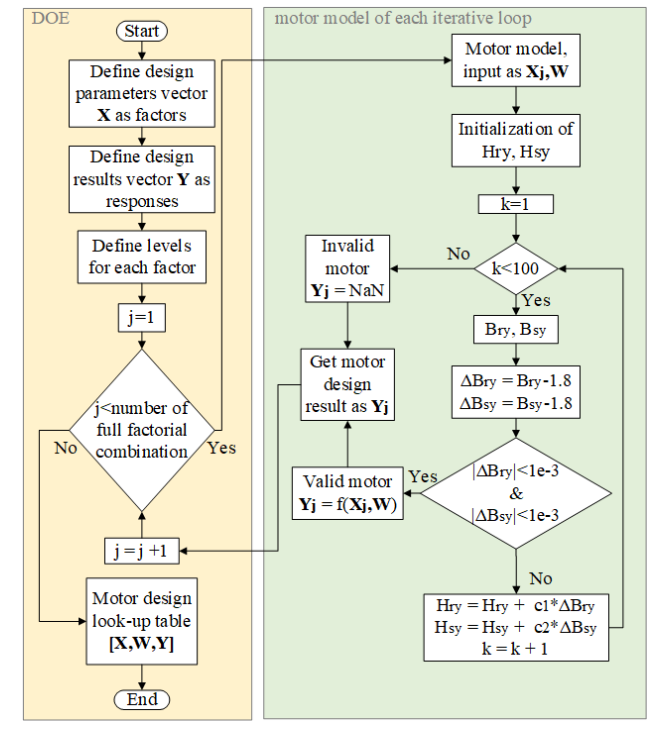


FIG 3. Design algorithm

3.2. Results Analysis

In this paper, the definition of levels for design parameters ${\bf X}$ is presented in Tab. 1

Name	Values
r_1	$[20,40,60,80,100,120,140,160,180,200] \times 10^{-3}$
K_{LD}	[0.1, 0.3, 0.5, 0.7, 0.9, 1, 1.5, 2, 2.5, 3]
H_{ag}	$[5, 10, 15] \times 10^{-3}$
H_{pm}	$[5, 10, 15] \times 10^{-3}$
H_{wd}	[5, 10, 15]×10 ⁻³
Ω_m	[10, 20, 30] $\times 10^3$
\overline{J}	[5, 10, 15] $\times 10^6$
$\overline{N_{pp}}$	[3, 4, 5]
$\overline{N_t}$	[5, 15, 25]

TAB 1. Definition of levels for design parameters

3.2.1. Study on the relationship between motor torque and motor geometry

To study the relationship between motor torque and motor geometry, an auxiliary variable V_r is defined to represent the volume of the cylindrical rotor. It is calculated as:

$$(37) V_r = \pi r_3^2 L$$

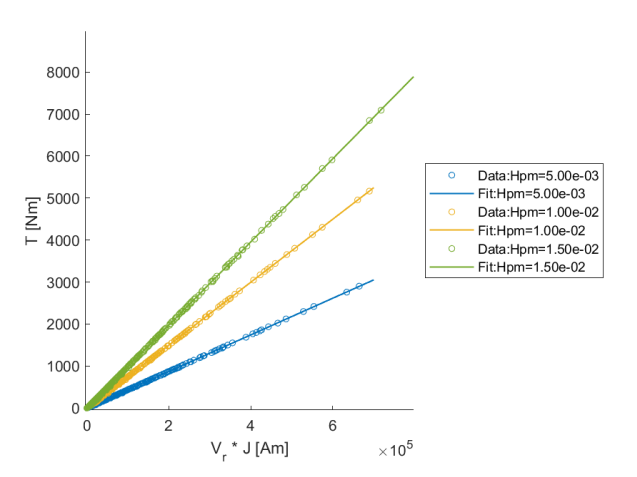


FIG 4. Typical relationship between motor torque and motor geometry with varying height of permanent magnets

In this study, r_1 , K_{LD} , Ω_m , J, N_{pp} , and N_t are treated as uncontrolled variables, while $H_{ag},\,H_{pm},\,{\rm and}\,\,H_{wd}$ are treated as controlled variables. In each study case, the value of the uncontrolled variables is allowed to vary freely, while the controlled variables remain constant. The typical relationship between motor torque and motor geometry is shown in Fig. 4. In this specific study, the controlled variables are set to $H_{ag} = 10$ mm and $H_{wd} = 10$ mm, while the controlled variable H_{pm} is varied between 5mm and 15mm, as defined by the full factorial levels. Each point in the figure represents a design result from the algorithm. It is observed that for each value of \mathcal{H}_{pm} , the motor torque has a linear relationship with the factor $V_r \cdot J$, indicating that motor torque is proportional to the cylinder rotor volume and the winding current density. In other words, to double the motor design torque, one could either double the motor length L, double the winding current density J, or increase the rotor outer radius r_3 by a factor of $\sqrt{2}$. The reason for this linear relationship between motor torque and the factor $V_r \cdot J$ can be explained by Esson's Rule [10]. According to this rule, motor power is proportional to the rotational speed of the motor, the $D_{is}^2 l_e$ factor, and the peak fundamental component of the AC surface current density K_{s1} , as follows:

$$(38) P_m \propto \Omega_m D_{is}^2 l_e K_{s1}$$

The D_{is} refers to the inner diameter of the stator, and l_e is the effective length of the stator, which is equal to L in this paper. Since the airgap height is relatively small, the $D_{is}^2 l_e$ factor can be approximated as the cylindrical rotor volume V_r .

$$(39) V_r \propto D_{is}^2 l_e$$

The peak fundamental component of the AC surface current density $K_{\rm s1}$ is proportional to the winding current density J, as follows:

$$(40) J \propto K_{s1}$$

According to equation (15), power divided by speed gives the torque. Therefore, the motor torque is proportional to the product of the cylindrical rotor volume and the winding current density:

$$(41) T \propto V_r \cdot J$$

The linear polynomial curve fitting is applied to each condition of H_{pm} in Fig. 4. It is observed that the slope of the

linear curve has a positive correlation with the design variable H_{pm} , indicating that, to produce the same amount of torque, a larger height of the permanent magnet results in a smaller required motor volume. Similar analyses have been conducted with the controlled variables H_{ag} and H_{wd} , and the analysis results are presented in Tab. 2. In the table, the symbol "+" denotes a positive correlation, and the symbol "-" denotes a negative correlation.

	H_{ag}	H_{pm}	H_{wd}
Slope	-	+	+

TAB 2. Correlation of the slopes in the fitted linear polynomial curve with varying values of controlled variables in the relationship between motor torque and motor geometry

3.2.2. Study on the relationship between motor torque and motor mass

Since the total motor mass includes both the stator and rotor components, in this study, the variables $H_{wd},\,H_{pm},\,H_{ag},\,J,$ and N_{pp} are treated as controlled variables, while r_1 , K_{LD} , Ω_m , and N_t are treated as uncontrolled variables. The number of pole pairs N_{pp} is included as a controlled variable due to its influence on the height of the stator yoke. The typical relationship between motor torque and motor mass is shown in Fig. 5. In this specific study case, the controlled variables are set to $H_{ag}\,=\,10\mathrm{mm},\;H_{pm}\,=\,10\mathrm{mm},\;H_{wd}\,=\,10\mathrm{mm},$ and $J = 5\text{A/mm}^2$, while the controlled variable N_{pp} is varied from 3 to 5. It is observed that the relationship between motor torque and motor mass follows a linear trend, with the slope of the fitted linear polynomial curve showing a positive correlation with N_{pp} . The reason for this positive correlation is the inverse relationship between N_{pp} and the stator yoke height H_{sy} . According to equations (34) and (36), increasing the number of pole pairs N_{pp} reduces the per-half-pole magnetic flux in the stator yoke, thereby reducing H_{sy} when the peak magnetic flux density $B_{sy.max}$ is kept constant in the design.

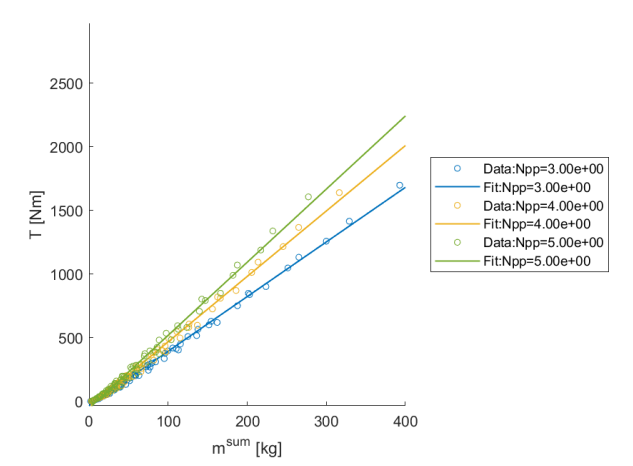


FIG 5. Typical relationship of motor torque and motor mass with varying number of pole pairs

Similar to the previous analysis of the relationship between motor torque and motor geometry, the correlation of the slopes in the fitted linear polynomial curve with varying values of controlled variables in the relationship between motor torque and motor mass is presented in Tab.3.

	H_{ag}	H_{pm}	H_{wd}	J	Npp
Slope	-	+	+	+	+

TAB 3. Correlation of the slopes in the fitted linear polynomial curve with varying values of controlled variables in the relationship between motor torque and motor mass

3.2.3. Study on the relationship between motor power and motor efficiency

In this study, H_{wd} , H_{pm} , H_{ag} , J, and N_{pp} are treated as controlled variables, while $r_1,\ K_{LD},\ \Omega_m,$ and N_t are treated as uncontrolled variables. The typical relationship between motor power and motor efficiency with varying height of permanent magnets is shown in Fig. 6. In this specific study case, the controlled variables are set to $H_{ag} = 10$ mm, $H_{wd} = 10$ mm, J = 5A/mm², and $N_{pp} = 4$. It is observed that the relationship between motor power and motor efficiency exhibits a "J" shape, where efficiency has a positive correlation with motor power in the low power range and a slight negative correlation in the high power range. Two auxiliary parameters, the knee point efficiency η_{max} and the maximum motor power $P_{m.max}$, are defined to describe the "J" shape curve. The knee point efficiency is the highest efficiency the "J" shape curve reaches, typically around the knee point. The maximum motor power is the highest design power the motor can achieve under specific controlled design variable conditions. Both η_{max} and $P_{m.max}$ are marked in Fig. 6 for $H_{pm}=5 \mathrm{mm}$ as an example. It is observed that both η_{max} and $P_{m.max}$ show an overall positive correlation with H_{pm} . For η_{max} , this positive correlation is more pronounced when \mathcal{H}_{pm} is relatively small, while it becomes less significant as H_{pm} increases. As previously discussed in Fig. 4, motor torque T has a positive correlation with H_{pm} , which explains why $P_{m.max}$ similarly exhibits a positive correlation with H_{pm} .

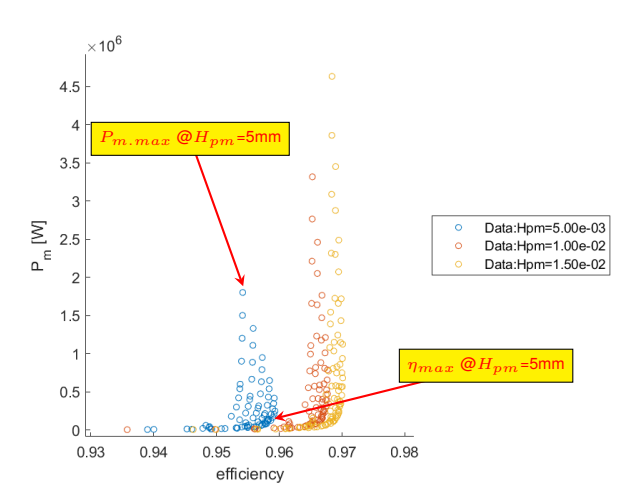


FIG 6. Typical relationship between motor power and motor efficiency with varying height of permanent magnets

For all other controlled variables, the relationship between motor power and motor efficiency similarly follows a "J" shape curve. The analysis of η_{max} and $P_{m.max}$ with varying values of the controlled variables in the relationship between motor power and motor efficiency is summarized in Tab. 4, where the symbol "=" indicates that the variable is relatively insensitive to changes.

	H_{ag}	H_{pm}	H_{wd}	J	N_{pp}
η_{max}	=	+	+	+	-
$P_{m.max}$	-	+	+	+	=

TAB 4. Correlation of the η_{max} and $P_{m.max}$ in J shape curves with varying values of controlled variables in the relationship between motor power and motor efficiency

A typical relationship between motor power and motor efficiency with varying air gap height is shown in Fig. 7, where the controlled variables are set to $H_{pm}=10$ mm, $H_{wd}=10\,$ mm, J=5 A/mm², and $N_{pp}=4$. For the controlled variable H_{ag} , its negative correlation with $P_{m.max}$ is due to the corresponding negative correlation with motor torque T. Additionally, the relationship between H_{aq} and η_{max} shows a slightly negative, yet insignificant correlation, indicating insensitivity. It is observed that η_{max} for different H_{ag} values occurs in a similar low power range. Based on the negative correlation between H_{ag} and the curve slope concluded in Tab. 2, the similar power output for different H_{aq} motor designs is achieved through adjustments in the motor's geometry, facilitated by changes in the uncontrolled variables. A larger air gap generally leads to increased windage losses. Furthermore, a larger air gap results in a weaker magnetic flux density, reducing the stator yoke volume and, subsequently, core losses. In the design parameter range defined in this paper, these complex influences lead to an overall insensitive correlation between H_{ag} and η_{max} .

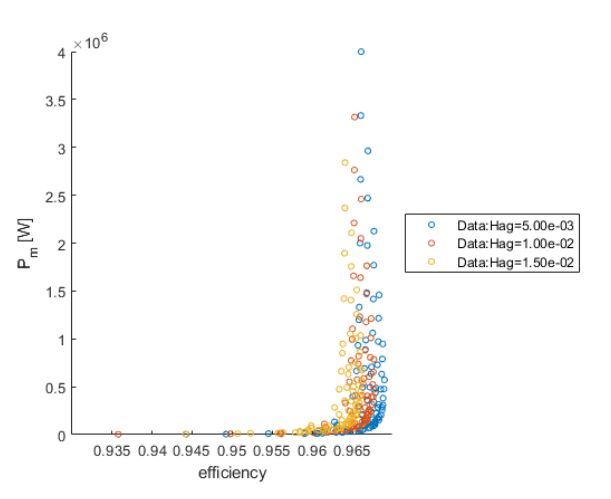


FIG 7. Typical relationship between motor power and motor efficiency with varying height of air gap

A typical relationship between motor power and motor efficiency with varying numbers of pole pairs is shown in Fig. 8, where the controlled variables are set to $H_{ag}=10 \mathrm{mm}$, $H_{pm}=10 \mathrm{mm}$, $H_{wd}=10 \mathrm{mm}$, and $J=5 \mathrm{A/mm}^2$. According to equation (25), a larger number of pole pairs results in a higher frequency, which in turn leads to increased core losses. As a result, N_{pp} has a negative correlation with the η_{max} .

4. CONCLUSION

This paper investigates the design of a case-mounted electrical motor for a counter-rotating hybrid electrical compressor, focusing on how various design parameters affect motor performance. A motor design algorithm based on full factorial experiments was developed, resulting in a look-up table that serves as an interface for other design disciplines. The study reveals that motor torque and motor geometry are lin-

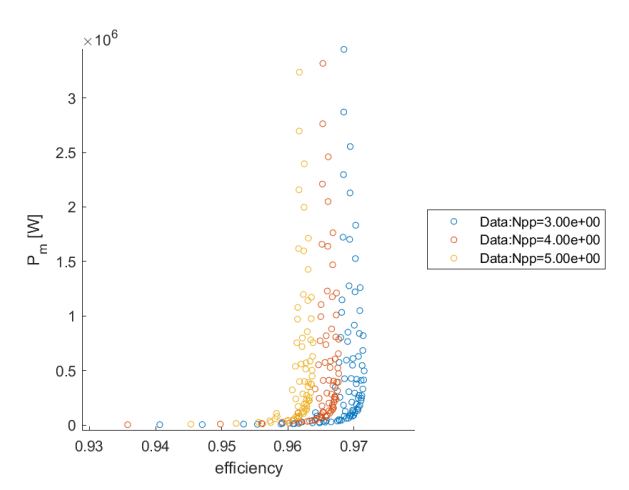


FIG 8. Typical relationship between motor power and motor efficiency with varying number of pole pairs

early related through the factor $V_r \cdot J$. To achieve a designed torque increase by a factor of two, either the motor length must be doubled or the rotor outer radius r_3 increased by a factor of $\sqrt{2}$. Additionally, the slope of the linear relationship between torque and geometry positively correlates with the height of the permanent magnets H_{pm} and the height of the windings H_{wd} , while negatively correlating with the height of the air gap H_{aq} . This suggests that motors with larger H_{pm} and H_{wd} , and smaller H_{ag} , are more compact for the same amount of designed torque. The relationship between motor torque and motor mass also shows a linear trend. To produce the same designed torque, motors with larger H_{pm} , H_{wd} , winding current density J, and number of pole pairs N_{pp} , or smaller H_{aq} , are lighter in weight. Regarding motor power and motor efficiency, the relationship is more complex and exhibits a "J" shape. Within the defined design parameters, the peak efficiency is higher at moderate power levels when H_{pm} , H_{wd} , and J are larger, or N_{pp} is smaller. Furthermore, the maximum designed motor power increases with larger H_{pm} , H_{wd} , and J, or smaller H_{ag} .

5. ACKNOWLEDGEMENTS

This work is funded by the BMWK (Federal Ministry for Economic Affairs and Climate Action of Germany) through Luftfahrtforschungsprogramm-VI (Grant number: 20E2111C).

References

- [1] Patrick C. Vratny, Sascha Kaiser, Arne Seitz, and Stefan Donnerhack. Performance investigation of cycleintegrated parallel hybrid turboshafts. *Journal of Engi*neering for Gas Turbines and Power, 139(3):031201, 09 2016. ISSN: 0742-4795. DOI: 10.1115/1.4034498.
- [2] Philipp Maas, Christopher Warsch, Raoul Böck, Moritz Kolb, and Arne Seitz. Pre-design investigation of a propulsion system with compressor electric drive. In DLRK 2024 - Deutscher Luft- und Raumfahrtkongress, 2024.
- [3] Jan Nittka, Mücahit Akkaya, Nicolai Neumann, and Dieter Peitsch. Aerodynamic pre-design and performance evaluation of counter rotating hybridised compressor concepts - modelling approach. In DLRK 2024 - Deutscher Luft- und Raumfahrtkongress, 2024.

- [4] Lucas Schreer and Volker Gümmer. Preliminary thermal management system design for cycle-integrated parallel hybrid compressors. In DLRK 2024 - Deutscher Luft- und Raumfahrtkongress, 2024.
- [5] Yinghui Yang and Georg Möhlenkamp. Analytical model for magnetic field distribution and electromagnetic characteristics analysis of permanent magnet synchronous motor with toroidal winding stator and sinusoidal halbach array rotor. *IET Conference Proceedings*, pages 210–217(7), June 2024. DOI: 10.1049/icp.2024.2159.
- [6] Jacek Gieras. PERMANENT MAGNET MOTOR TECHNOLOGY: DESIGN AND APPLICATIONS, chapter Appendix B, pages 565–576. CRC Press, 01 2010. ISBN: 978-1-4200-6440-7.
- [7] Dheeraj Bobba, Zhaoxi Yao, James Swanke, Raphael Mandel, Patrick McCluskey, Thomas Jahns, and Bulent Sarlioglu. Multi-physics based analysis and design of stator coil in high power density pmsm for aircraft propulsion applications. In 2021 AIAA/IEEE Electric Aircraft Technologies Symposium (EATS), pages 1–9, 2021. DOI: 10.23919/EATS52162.2021.9704820.
- [8] D. Lin, P. Zhou, W.N. Fu, Z. Badics, and Z.J. Cendes. A dynamic core loss model for soft ferromagnetic and power ferrite materials in transient finite element analysis. *IEEE Transactions on Magnetics*, 40(2):1318– 1321, 2004. DOI: 10.1109/TMAG.2004.825025.
- [9] Victor Johannes Bahrs, Martin Staggat, and Lars Enghardt. Analytical model for electric machine sizing in electrified aviation. In *Deutscher Luftund Raumfahrtkongress 2022*, December 2022. DOI: 10.25967/570099.
- [10] Thomas A. Lipo. Introduction to AC Machine Design, chapter 6, pages 251–303. John Wiley & Sons, Ltd, 2017. ISBN:9781119352181. DOI: https://doi.org/10.1002/9781119352181.ch6.

CC BY-NC-ND 4.0